한국동력기계공학회지 제17권 제5호 pp. 100-111 2013년 10월 (ISSN 1226-7813)
Journal of the Korean Society for Power System Engineering, Vol. 17, No. 5, pp. 100-111, October 2013
Research paper

Positioning Accuracy on Robot Self-localization by Real-time Indoor Positioning System with SS Ultrasonic Waves

Akimasa Suzuki*† , Ken Kumakura**, Daisuke Tomizuka**, Yoshinobu Hagiwara***, Youngbok Kim****, and Yongwoon Choi**

(received 22 September 2013, revised 05 October 2013, accepted 06 October 2013)

Abstract : Indoor real-time positioning for multiple targets is required to realize human-robot symbiosis. This study firstly presents positioning accuracy on an autonomous mobile robot controlled by 3-D coordinates that is obtained by a real-time indoor positioning system with spread spectrum (SS) ultrasonic signals communicated by code-division multiple access. Although many positioning systems have been investigated, the positioning system with the SS ultrasonic signals can measure identified multiple 3-D positions in every 70 ms with noise tolerance and error within 100 mm. This system is also robust to occlusion and environmental changes. However, thus far, the positioning errors in an autonomous mobile robot, controlled by these systems using the SS ultrasonic signals, have not been evaluated as an experimental study. Therefore, a positioning experiment for trajectory control is conducted using an autonomous mobile robot and our positioning system. The effectiveness of this positioning method for robot self-localization is shown, from this experiment, because the average control error between the target position and the robot's position at 29 mm is obtained.

Key Words : Real-time Indoor Positioning System, Spread Spectrum Ultrasonic Waves, Autonomous Mobile Robot, Self-localization, 3-D Coordinates

1. Introduction

The fields of application of position information have expanded in tandem with advancements in our information-driven society. The position information is required to realize the self-localization of autonomous mobile robots for human-robot symbiosis such as cooperative working between robots and humans. In these cases, the moving targets have to be continuously measured with high accuracy. The positions of each target have to be also identified. We also expect to the positioning information as data log to analyze their movement, such as a factor or tendency of the positioning error on the control, for the human-robot symbiosis.

Many positioning systems are actively researched. The positioning system to achieve the self-localization of the robots, for obtaining coordinates using the infrastructure, is more robust

*† Akimasa Suzuki (corresponding author) : Department of Software and Information Science, Iwate Prefectural University, Japan.
** Ken Kumakura, Daisuke Tomizuka, and Yongwoon Choi: Department of Engineering, Soka University, Japan.
*** Yoshinobu Hagiwara: National Institute of Informatics, Japan.
**** Youngbok Kim: Pukyong National University, Korea.
E-mail: kpjiwoo@pknu.ac.kr, Tel : 051-629-6197

to environmental changes than the other systems using sensors mounted on the robots. This system enables to apply for the positioning of not only robots but also humans.

Therefore, the systems that use the infrastructure devices of such as pseudolites[1] or radio waves[2] have been investigated. When compared to other methods, the use of ultrasonic waves is inexpensive, highly accurate, and robust to occlusion and illumination changes. However, these systems have weak noise resistance and take a longer period of time to acquire data because the use of Time Division Multiple Access (TDMA) with on-off keying becomes cumbersome as the number of objects being measured increases. Spread spectrum (SS) ultrasonic waves have been investigated[3,4] to overcome these drawbacks.

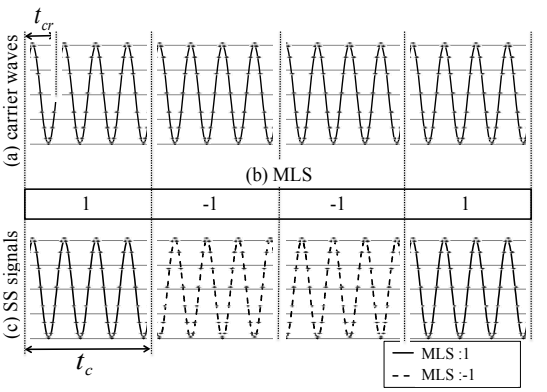

Fig. 1 Ultrasonic signals generated in the transmitter units (a) carrier waves and (c) SS signals multiplied to (b) MLS.

Previously, we have also proposed an inexpensive and accurate real-time 3-D positioning system with SS ultrasonic signals, using an all-purpose transducer, low-power FieldProgrammable Gate Array (FPGA), and a small microprocessor. We have also targeted the system within every 80 ms at less than 100 mm to overcome the self-localization. For applying for robots, which perform the self-localization and the service corporation, previous studies on the component technologies of this system such as robustness to moving speed[5], measurement precision of all-purpose transducers[6], positioning errors in indoor environments[7,8], and real-time hardware computation for correlation calculations[9] have been discussed in offline processing..

However, thus far, positioning accuracy on an autonomous mobile robot has not been discussed in an experimental study when this trajectory control has been conducted. Therefore, in this study, a running experiment using an autonomous mobile robot and this positioning system for a 4000 mm by 4000 mm experimental space is conducted. The effectiveness of this positioning method for the cooperative working between robots and humans and the data logger for analyzing the movements is shown, from this experiment, because the average positioning error at 27 mm is obtained in case that the robot is only controlled at rotating points and around target subgoals.

In this study, next chapter provides an overview of our positioning method, including the modulation and calculation method using CDMA by continuous SS signals. Chapter 3 covers the measurement accuracy of our positioning system in an experimental environment. Chapter 4 deals with accuracy on the error of the distance from target subgoal, and with a distribution of measurement position in case of trajectory control using an autonomous mobile robot in this positioning environment.

2. Real-time Indoor 3-D Positioning System using Continuous SS Ultrasonic Signals

2.1 SS Ultrasonic Signals

In our indoor positioning system, the SS signals

are modulated by binary phase shift keying (BPSK) using a maximum length sequence (MLS) —a pseudorandom sequence—as used in the direct sequence (DS) method. Although an MLS of "0" or "1" is generated by the shift register, we have used the value of "-1" instead of "0" to facilitate signal processing. Fig. 1 shows the received SS signal. As shown in Fig. 1, the signals corresponding to "1" and "-1" are plotted by solid and dashed lines, respectively. Each dot in Fig. 1 denotes a "sampling"; the number of samples including one period worth of carrier waves is selected to be four. Here, the chip length is defined as the time required to describe the one-chip worth of the MLS. The chip length can be also defined as $t_c = 4/f$, using the carrier frequency $f = 1/t_{cr}$. The bit length of this shift register governs the calculation result and signal to noise ratio. In our system, a 9-bit shift register was utilized to achieve real-time correlation calculations with a high S/N ratio. The length of the sequence becomes 2^9 - 1 = 511 bits (chips) periods. Thus, the MLS period can be calculated as $T = 511 \times t_c$. In this system, an SS signal is generated continuously by carrier waves at a frequency of 40 kHz, and the period time T is 51100 μs.

2.2 Signal Detection using Continuous Ultrasonic Signals

The measurement position is calculated from over three certain distances between the transmitters and the receiver. Signal detection is performed in a receiver unit to obtain a distance. This positioning calculation and signal detection can be realized using a slow microprocessor (AKI-H8 3052F) and Altera Cyclone (EP1C 6Q240C6) as a low-power FPGA, respectively.

Fig. 2 shows the procedure for the signal detection. The signals from the transmitter are detected from the calculated correlation values. The correlation calculation is performed between the received signals and the replica signals within one cycle of the MLS as shown in Fig. 2. In signal detection, the correlation values are calculated for every one sampling time. From this calculation, the peak values cor_{peak} are detected by the self-correlation characteristics of the MLS when the transmitted signal is received. Otherwise, the correlation values are obtained at approximately $\frac{cor_{peak}}{511}$. Signal detection results in a time-of-flight (TOF) from the time when the top of the MLS is transmitted by the transmitter to the time of peak detection. The top of the MLS is transmitted from the transmitter during the transmission timing, as shown in Fig. 2. The measurement distance between the transmitter and the receiver is calculated from the TOF. The peaks can be obtained at each period , as shown in Fig. 2 because of the periodicity on MLS. In our transmitting system, the transmission timing shown in Fig. 2 is synchronized with this period. The TOF can be continuously obtained at $20 \times T$ s interval.

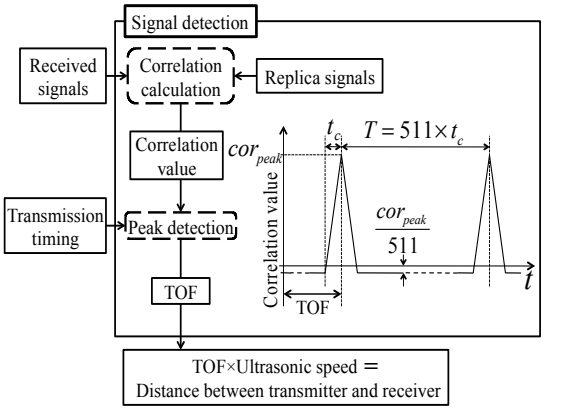

Fig. 2 Signal detection for measuring the distance.

2.3 Real-time Positioning Calculation using the Least-Squares Method

More than three distances from the transmitters to the receiver on a target are required to measure the position, since are three coordinates (x, y, z) that must be calculated. The more distances are measured, the higher accurate position is obtained. Thus, more than three transmitters are required, each generating different MLS codes with low cross-correlation, allowing for division positioning. Coordinates on a receiver are calculated from simultaneous equations of the different distances and the known coordinates of the transmitters. We could use a repetitive Newton–Raphson method to solve these equations in analogy to GNSS[10], however the clock bias term can be removed from the positioning calculation because the proposed system calculates TOF using timings sent by the transmitter.

Our indoor positioning system calculation is outlined in Fig. 3. A target position Rx is calculated from the coordinates of three transmitters (Tx_1, Tx_2, and Tx_3), and the distances obtained from TOFs. A distance, r_i (r_1, r_2 and r_3 in Fig. 3), between $Tx_i(x_i, y_i, z_i)$ and $Rx(x, y, z)$ is

$$r_i = \sqrt{(x_i - x)^2 + (y_i - y)^2 (z_i - z)^2} \tag{1}$$

where $Rx(x, y, z)$ and $Tx_i(x_i, y_i, z_i)$ are defined as the true coordinates of a receiver, and the i-th arbitrary coordinates of a transmitter, respectively. The subscript i denotes the transmitter number and takes values 1, 2, ..., n, where n is greater than 3. We write $Rx(x, y, z)$ as

$$\begin{aligned} x &= x_0 + \triangle x, \\ y &= y_0 + \triangle y, \\ z &= z_0 + \triangle z \end{aligned} \tag{2}$$

where $Rx_0(x_0, y_0, z_0)$ are the initial coordinates which the positioning system gives. $\triangle x$, $\triangle y$, $\triangle z$ are the x, y and z components of correction distance between the initial coordinates and $Rx_0(x_0, y_0, z_0)$, respectively. The distance r_{0i} between the initial coordinates and the i-th transmitter is

$$r_{0i} = \sqrt{(x_i - x_0)^2 + (y_i - y_0)^2 (z_i - z_0)^2} \tag{3}$$

Thus the distance $\triangle r_i$ between $Rx(x, y, z)$ and $Rx_0(x_0, y_0, z_0)$ is given by

$$\triangle r_i = r_i - r_{0i} \tag{4}$$

Partial differential coefficients α_i, β_i and γ_i can be evaluated from $\triangle r_i$ and the x, y, and z components of $Rx_0(x_0, y_0, z_0)$, respectively. $\triangle r_i$ can be also expressed as (5) using α_i, β_i and γ_i:

$$\begin{pmatrix} \triangle r_1 \\ \vdots \\ \triangle r_i \end{pmatrix} = \begin{pmatrix} \alpha_1 & \beta_1 & \gamma_1 \\ \vdots & \vdots & \vdots \\ \alpha_i & \beta_i & \gamma_i \end{pmatrix} \begin{pmatrix} \triangle x \\ \triangle y \\ \triangle z \end{pmatrix} \tag{5}$$

We define vector $\triangle R$, matrix A, vector $\triangle X$, and vector ε

$$\triangle R = \begin{pmatrix} \triangle r_1 \\ \vdots \\ \triangle r_i \end{pmatrix} \tag{6}$$

$$A = \begin{pmatrix} \alpha_1 & \beta_1 & \gamma_1 \\ \vdots & \vdots & \vdots \\ \alpha_i & \beta_i & \gamma_i \end{pmatrix} \tag{7}$$

$$\triangle X = \begin{pmatrix} \triangle x \\ \triangle y \\ \triangle z \end{pmatrix} \tag{8}$$

$$\varepsilon = \begin{pmatrix} \varepsilon_1 \\ \vdots \\ \varepsilon_i \end{pmatrix} \tag{9}$$

where ε is the vector of the measurement errors shown in Fig. 3. Equation (5) can be denoted by

$$\triangle R = A \triangle X + \varepsilon \tag{10}$$

using (6), (7), (8), and (9). Let us consider the solution such that the minimum value of is obtained using a least squares method[10]. The sum of ε squared, defined as f, is

$$\begin{aligned} f &= \sum_{j=1}^{i} \varepsilon_j^2 = \varepsilon^T \varepsilon \\ &= (\triangle R - A\triangle X)^T (\triangle R - A\triangle X) \\ &= \triangle R^T \triangle R - 2\triangle R^T A \triangle X + \triangle X^T (A^T A) \triangle X \end{aligned} \tag{11}$$

In order to minimize f the partial differential of (11) is carried out with respect to $\triangle X$,

$$\frac{\partial f}{\partial \triangle X} = -2\triangle R^T A + 2\triangle X^T (A^T A) = 0 \tag{12}$$

The location of extrema is calculated using

$$\triangle X^T (A^T A) = \triangle R^T A \tag{13}$$

$\triangle X$ is obtained by deformation of (13).

$$\triangle X = (A^T A)^{-1} A^T \triangle R \tag{14}$$

Thus, $Rx(x, y, z)$ is:

$$Rx(x, y, z) = Rx_0(x_0, y_0, z_0) + \triangle X \tag{15}$$

When $Rx_0(x_0, y_0, z_0)$ is close to $Rx(x, y, z)$, we obtain a highly precise calculation. Therefore, highly precise positioning is maintainable by setting the obtained valued of $Rx(x, y, z)$ of to b $Rx_0(x_0, y_0, z_0)$ in the subsequent calculation.

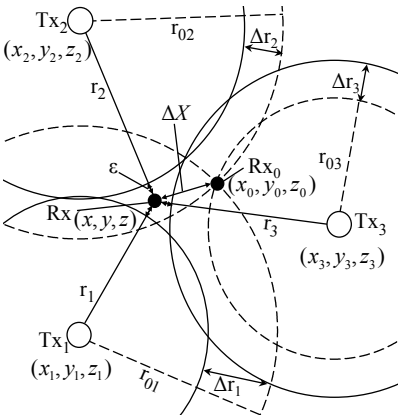

Fig. 3 Position calculation method using the least-squares method.

3. Positioning Accuracy and Measurable Area of the Positioning System in a Room

3.1 Experimental Environment in a Positioning Room

The positioning accuracy of our indoor positioning system in the case of a stationary target are evaluated under an experimental environment, as shown in Fig. 4. Fig. 4 (a) shows the overview of a given space that has four transmitters, namely, as Tx_1, Tx_2, Tx_3, and Tx_4. Although the coordinates are obtained from over three transmitters, we install the four transmitters in this environment to measure accurately and robustly to the occlusion. The heights of Tx_1 to Tx_4 were measured using a laser range finder since the height the floor to the roof differed over the area of the experiment, as shown in Fig. 4(a). Their heights were 2732, 2727, 2739 and 2727 mm, respectively.

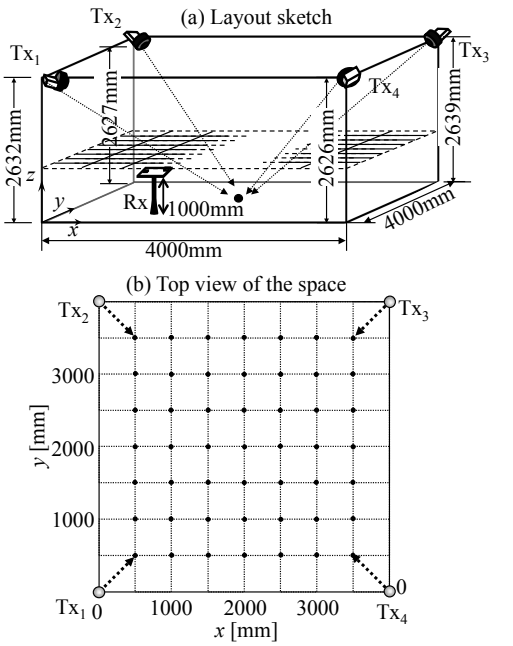

Fig. 4 Experimental environment for investigating the accuracy using continuous SS ultrasonic signals.

Fig. 4 (b) shows the measurement positions. We define an origin of rectangular coordinates system as the floor point at Tx_1. As shown in Fig. 4 (b), 49 points are measured using a receiver at 1000-mm height, as shown in Fig. 4 (a). The transmitters are directed to the center of the area, at (2000, 2000, 0) mm, as shown in Fig. 4. In this evaluation, a transmitter with a closed-type aperture (PC40-18S, Nippon Ceramic Co., Ltd.) and a "Mini" SiSonic™ ultrasonic receiver (SPM0404UD5, Knowles) are used as general-purpose ultrasonic transducers. The operating voltage and current of this receiver are up to 3.6 V and 0.25 mA, respectively. The transmitter voltage amplitude is 10.5 Vp-p. The positioning accuracy is measured 20 times at each of the 49 points, respectively. The result was evaluated using the Euclidean distance as above. As such, the positioning error ep_{rms} is defined using the measured distances x_m, y_m, z_m and true distances x, y, z, corresponding to each coordinate:

$$ep_{rms} = \sqrt{(x_m - x)^2 + (y_m - y)^2 (z_m - z)^2} \qquad (16)$$

The average value of the Euclidean distance is defined as the positioning error at each point. The positioning error and calculation time are discussed as factors relating to the usefulness of the system.

3.2 Positioning Accuracy and Time of the Positioning System using SS ultrasonic Signals for an Stationary Target

As shown in the results of a stationary target, the positions at all the measurement points are obtained. In this evaluation, the maximum electric power of the FPGA and the microprocessor became 219.7 mW and 300 mW, respectively. Fig. 5 shows a top view of the positioning accuracy for measurement points. The scale at the top shown in Fig. 5 shows the range for a positioning error at each measurement point. For example, ⑤ at (500, 500, 1000) corresponds to a range of positioning errors between 40 mm and 50 mm.

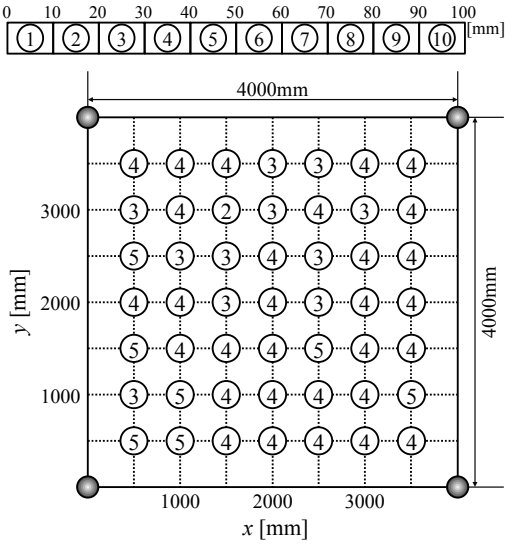

Fig. 5 Distribution of positioning errors in the indoor positioning system using SS ultrasonic waves.

It is observed from this evaluation, that the average positioning error at all the points is 35 mm. Moreover, the standard deviation in all measurement points is obtained at approximately 7 mm. Although most of the measurement errors occur because of the simultaneous CDMA using the continuous signals instead of the conventional TDM, the measurement error at each positioning point is up to 50mm, as shown in Fig. 5. We have used transmitters and a receiver with wide directional characteristics and can obtain the high accurate distances in wide area. Thus, from the distribution shown in Fig. 5, we cannot confirm the liability of the positioning errors at each point, even though the error attributed to each position should have occurred because of the dilution of precision[7].

Table 1 The maximum, minimum and average time of calculation and response.

	Maximum [ms]	Minimum [ms]	Average [ms]
Calculation time	15	11	12
Response time	72	56	65

Table 1 lists the maximum time, minimum time, and average time of the positioning calculation using our proposed method. The response time-cycle, which is an interval from the arrival of the electrical signal to the positioning acquisition, is also given. As such, the response period contains the calculation period. The maximum, minimum and average times of the calculation time were 15, 11 and 12 ms, respectively. That is, the proposed method can calculate positions in less than 20 ms. Moreover, the maximum, minimum and average times of response were 72, 56 and 65 ms. Therefore, we can obtain a position in a response time of less than 80 ms, even though we use a relatively slow H8 processor. It can be observed from these two results on accuracy and time that this positioning system achieves the required positioning accuracy for realizing the self-localization of the autonomous robots.

4. Control Experiment with Robot using the Positioning System

4.1 Experimental Setting for the Trajectory Control

The cooperative working between robots and humans and the data logger for analyzing their movements require the positioning system which can be used for the robot self-localization. For evaluating whether the robot self-localization is accurately realized usingour indoor real-time positioning system with the SS ultrasonic waves, a trajectory control of an autonomous mobile robot is conducted using the 3-D coordinates obtained from this system. Fig. 6 shows the outline of this experiment. In this experiment, as shown in Fig. 6, Tx_1 to Tx_4 are located similar to the experiment shown in Fig. 4. We also define the origin of the rectangular coordinates system as the floor point at Tx_1, similar to that shown in Fig. 4 (a). The positive directions from Tx_1 toward Tx_4 and Tx_2 are applied as the x- and y-axis respectively. Fig. 6 also shows the example of moving path at the *i*-th lap as a solid line, in case of moving for clockwise direction. A moving route for the robot is also shown in Fig. 6 as a dot line in case of moving for clockwise direction.

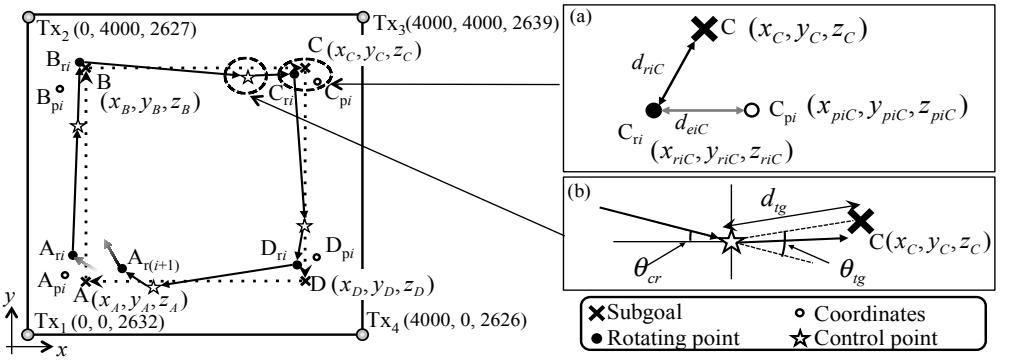

Fig. 6 Experimental outline of the trajectory control using an autonomous mobile robot.

If the robot travels for clockwise direction, the robot goes straight for 2000 mm and rotates at 90° to the right repeatedly. In the case of counterclockwise, the robot rotates to the left.. As shown in x-mark in Fig. 6, points $A(x_A, y_A, z_A)$, $B(x_B, y_B, z_B)$, $C(x_C, y_C, z_C)$, and $D(x_D, y_D, z_D)$ are applied as the subgoals where the robot rotates. X-y coordinates of the subgoals A to D are (1000, 1000), (1000, 3000) (3000, 3000), and (3000, 1000), respectively. As the initial setting, an autonomous mobile robot is installed at point A (1000, 1000, 0) in a direction parallel to the y-axis. In this experiment, the robot travels 5 laps on a carpet in the clockwise and the counterclockwise direction and in the alphabetical, and the reverse alphabetical order, respectively.

Fig. 6 (a) and (b) also indicate enlarged views around the subgoal of point C and the control point between Point B and C respectively. In this experiment, rotating points A_{ri} to D_{ri} shown in Fig. 6 as the black circles, are measured when the robot arrives from A to D where the robot rotates at a position located just underneath at P of the robot (See Fig. 7). We discuss the errors in the distances between the position of the robot and the subgoal with the coordinates obtained by our system. As shown in Fig. 6(a), d_{riA} to d_{riD}, and d_{eiA} to d_{eiD}, which are the distances on the *i*-th subgoal from A to D, denotes as the errors between the position of the robot and the subgoal, and between the position of the robot and the coordinate, respectively. In brief, d_{riA} to d_{riD} and d_{eiA} to d_{eiD}, mean positioning errors on the trajectory control of a robot, and the positioning error at our positioning system corresponding to Fig. 5, respectively.

4.2 Autonomous Mobile Robot with Wheels

In this experiment, a 2WD robot with a height of 1300 mm and a width of 550 mm is used. This robot is 70 kg weight. We describe the robot architecture and the mount position of ultrasonic transducer in Fig. 7. A receiver is mounted on a robot above middle point P, located between left and right wheel, as shown in Fig. 7. Here, the x- and y- coordinates of P (x_r, y_r) are defined as the position of the robot on the positioning area. The coordinates of the receiver should be (x_r, y_r, 1300) mm. As shown in Fig. 6, this position when the robot rotates is shown as A_{ri} to D_{ri}, which is denoted by black circles. In the both wheels, DC motors (Maxon RE36) and encoders (MR256) are installed.

4.3 Method for the trajectory control of this experiment

Points A_{pi} to D_{pi}, shown by the white circle in Fig. 6 denotes the coordinates where the robot rotates. These coordinates are obtained from our positioning system. Although trajectory control can be realized for 3-D movement using this coordinates, in this experiment, we use a simple controlling method for the 2WD robot without altitude control. When the autonomous mobile robot travels to the next subgoal A to D, distance d_{tg} and the angle for direction θ_{tg} are calculated using the measurement coordinates obtained from our positioning system (see Fig. 6(b)). For instance, d_{tg} and θ_{tg} at a position between points B and C in the *i*-th lap are obtained using the current direction θ_{cr} of the robot and coordinates obtained at the *i*-th lap of the current control point $(x_{piBC}, y_{piBC}, z_{piBC})$ and the subgoal C (x_C, y_C, z_c), defined as

$$d_{tg} = (x_c - x_{piB})^2 + (y_c - y_{piB})^2 \tag{17}$$

$$\theta_{tg} = \theta_{cr} - \tan^{-1}\frac{y_c - y_{piBC}}{x_c - x_{piBC}} \tag{18}$$

respectively, in this experiment. Here, θ_{cr} can be estimated using the measured coordinates of one before point. In this example, θ_{cr} is denoted using this measured coordinates $(x_{piB}, y_{piB}, z_{piB})$, where the robot rotates, as follows (19):

$$\theta_{cr} = \tan^{-1}\frac{y_{piBC} - y_{piB}}{x_{piBC} - x_{piB}} \tag{19}$$

Repeated trajectory control by the calculated control variable shown in (17) to (19) is desirable while the robot is traveling, to accurately reach the subgoal. In this experiment, however, the encoders in robot are only operated by the control variable at the rotating point and controling point around target subgoal, shown by the black circle and star mark in Fig. 6, respectively. Distances between the subgoal and this control point are approximately 500mm.

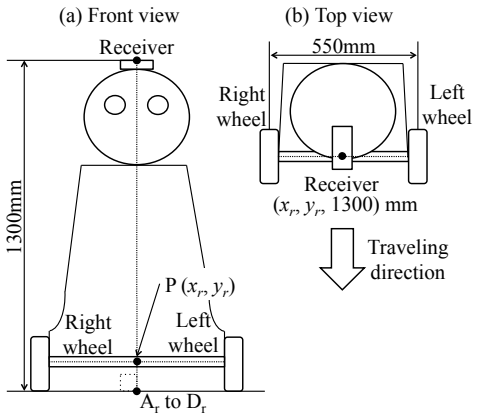

Fig. 7 Autonomous mobile robot for the trajectory control experiment.

4.4 Discussion on the Error of Distance

We describe the experimental result as summarized in Table 2 and Fig. 8. Table 2 ((a) and (b)) summarizes the average errors at (a) d_r between the subgoal (i.e., A, B in Fig. 6) and the rotating point of the robot (i.e., A_r, B_r in Fig. 6), and (b) d_e between the position of the robot and the coordinates. The distance errors d_r and d_e are approximated at the sampling time from measurement start to the signal detection and temperature T. The temperature at which this experiment is conducted is 25°C. Table 2 shows each average error in case that robot travels clockwise and counterclockwise direction. The errors of both clockwise and counterclockwise are also shown. It is observed from experimental result shown in Table 2, RMS positioning errors of d_r in the case of clockwise direction, counterclockwise direction, and the both were 27, 30, and 29, respectively. RMS positioning errors of d_e in the case of clockwise direction, counterclockwise direction, and the both were also obtained as 24, 34, and 29 mm, respectively.

Table 2 Average RMS errors of (a) d_r between the subgoal and the position of the robot and (b) d_e between the position of the robot and the coordinates.

	RMS error [mm]		
	Clock wise	Counter-clockwise	Both
(a) d_r (Subgoal − robot)	27	30	29
(b) d_e (Robot −coordinates)	24	34	29

Fig. 8 also shows the Euclidean distance errors obtained in real-time at the subgoal from A_1 to A_6, in the case of traveling in the (I) clockwise and (II) counterclockwise direction. As shown in Fig. 8 (I) and (II), the x-axis is from A_1 to A_6 and the y-axis is from low to high positioning error. As shown in Fig. 8 (a) and (b), the solid and gray lines represent the distance errors as d_r between the subgoal and the position of the robot, and (b) d_e between the position of the robot and the coordinates obtained using the system, respectively. In addition, the subgoal and the error in the distance are arranged in an ascending order on the x- and y-axis, respectively. For example, A_2 on the x-axis shown in Fig. 8 shows the measurement point A at 2nd lap.

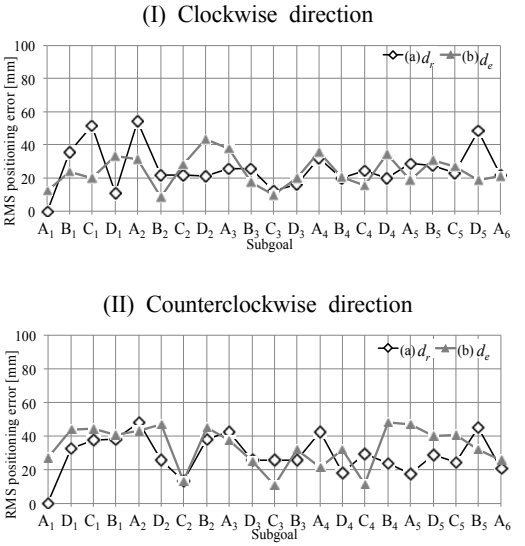

Fig. 8 RMS positioning error at distance (a) d_r between the subgoal and the position of a robot, and (b) distance d_e between the position of the robot and the coordinates on (I) clockwise and (II) counterclockwise direction.

At the point of A_1, d_r is axiomatically 0 mm, because we have mounted the robot at subgoal A_1 as the initial position. As can be observed from Fig. 8 and Table 2, we have confirmed that the error in d_e is similar to the result of Fig. 5. Therefore, our positioning system correctly works at this experiment. In addition, d_r presented almost the same tendency as that of d_e, because the coordinates obtained at the control point have the error as same as at rotating point, and affect trajectory control. Fig. 8 (I) and (II) show that the Euclidean distance errors of d_r shown in Fig. 8 (a) are within 60 mm at all the measurement points on the subgoals. The Euclidean distance error is not accumulated from the traveling route.

Although the robot was only controlled twice (at the rotating and the control point) whenever the robot travels to each subgoal, we could measure the average of positioning error between the robot and the subgoals within 60 mm. We

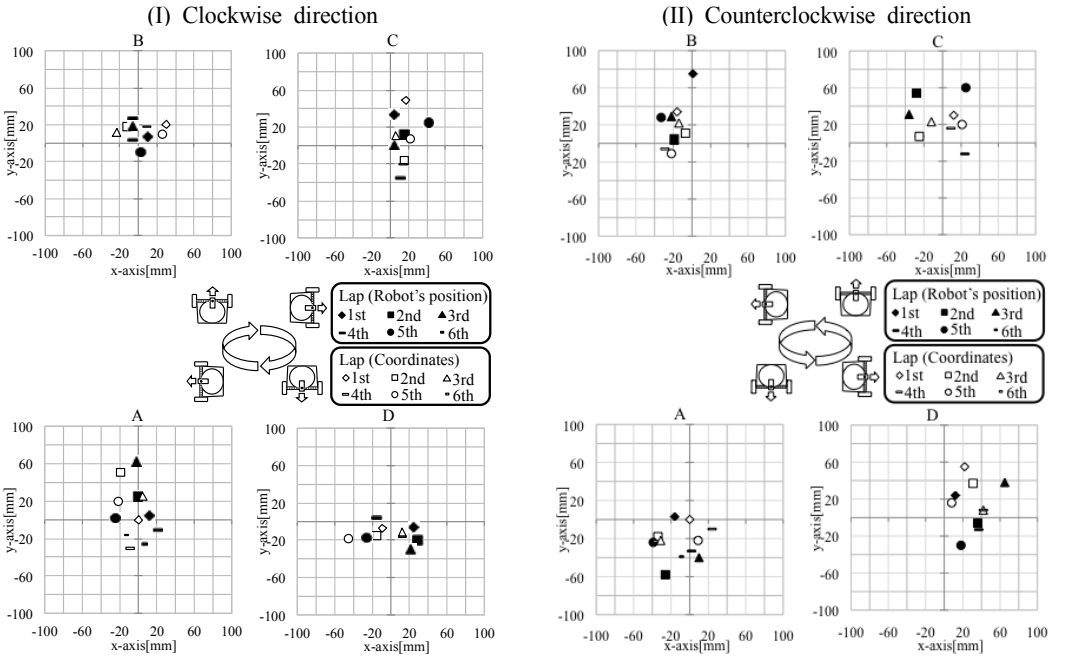

Fig. 9 Position of the robot and the coordinates obtained by our system on each (I) clockwise and (II) counterclockwise direction.

require a 100-mm or smaller positioning errors for accurate self-location recognition of robots and humans Thus, we expects to achieve the required accuracy for the trajectory control of a traveling robot using this positioning system.

4.5 Discussion on the Robot`s Position and Coordinates from Our System

Fig. 9 represents the measurement position of the robot and the coordinates obtained by our positioning system, when the robot reach each subgoal A to D. Fig. 9 (I) and (II) are the position in case of clockwise and counterclockwise direction, respectively.

The original points on Fig. 9 are the position of the subgoals, and errors on each lap are plotted. In Fig. 9, black and white marks represent the position of the robot and coordinates obtained from our system, respectively. The positions are measured before the robot rotates, and the posture of the robot on the measurement position is also shown in the center of Fig. 9 (I) and (II).

We can find from Fig. 9 that many measured positions on both robot's position and coordinates are plotted in front of subgoals. The traveling distance estimated by control values of the robot are more than true distance, because traveling distance is varied from friction between the robot and a floor. The coordinates obtained from our system are measured near the position of the robot, as shown in Fig. 9, although some coordinates are placed at approximately 40-mm far from the robot's position, owing to the ability of our positioning system. It is observed from this experiment that the trend of the positioning error on the robot can be obtained from our system with the error less than 40-mm. Therefore, we expect to realize data logger for analyzing the movements of a robot as tendency by using our positioning system.

5. Conclusions

In this study, to realize the cooperative working between robots and humans and the data logging for analyzing their movements, we have firstly discussed the positioning accuracy measured from the trajectory control using the real-time positioning system using SS ultrasonic waves from an experiment conducted on a traveling robot.

The positioning system, which we have been investigated, can measure the 3-D coordinates of the targets in every 70 ms and with an error within 5 cm using the all-purpose transducers with low-power devices. For investigating the positioning accuracy of a robot control, we have conducted an experiment using an autonomous mobile robot, which travels 5-lap via four subgoals in the clockwise and the counterclockwise direction in a measurement environment, respectively. It is observed from the experiment conducted for the trajectory control, that the coordinates of the robots are located at 29 mm with the average positioning error. This experimental result is similar to the positioning accuracy using the stationary target. We have also measured the positioning errors from the subgoals to the positions of the robot within an average of 29 mm, and a maximum within 60 mm, respectively, even though the coordinates are measured at rotating points and control point around subgoals.

Thus, the effectiveness of the proposed SS positioning system for robot self-localization is demonstrated. It is observed from this result that we expect to realize the cooperative working and the relal-time data logger for analyzing the movement of the robot and the human by using our positioning system. The service corporation for human-robot symbiosis using coordinates obtained from our positioning system can be also expected.

In further work, we will perform experiments for the self-localization of indoor flying robots at staircase using our positioning system.

Acknowledgement

This work was supported by the Basic Science Research Program funded by the Ministry of Education Science and Technology (2012R1A1A22039012). Also, this work was a part of the project titled: “The Development of Mooring Positioning Control System for Offshore Accommodation Barge” funded by the Ministry of Oceans and Fisheries.

References

1. J. E. Lee and S. G. Lee, 2010, "Indoor initial positioning using single clock pseudolite system", International Conference on Information and Communication Technology Convergence (ICTC), Jeju, pp. 575-578.
2. D. Manandhar and H. Torimoto, 2011, "Development of IMES Installation, Setup and Management System", Proceedings of the 24th International Technical Meeting of The Satellite Division of the Institute of Navigation, Portland, pp. 1507-1513.
3. M. Hazas and A. Ward, 2006, "Broadband Ultrasonic Location Systems for Improved Indoor Positioning", IEEE Transactions on Mobile Computing, pp. 536-547.
4. A. M. Aly Omar and A. S. Omar, 2005, "Spread Spectrum Ultrasonic Positioning System", The 2nd Workshop on Positioning, Navigation and Communication (WPNC’05) & 1st Ultra-Wideband Expert Talk (UET'05), Hanover, pp. 109-114.
5. Y. Itagaki, A. Suzuki, and I. Taketoshi, 2012, "Indoor Positioning for Moving Objects Using a Hardware Device with Spread Spectrum Ultrasonic Waves", International Conference on Indoor Positioning and Indoor Navigation (IPIN 2012), Sydney, pp. 1-6.
6. A. Yamane, I. Taketoshi, Y. W. Chio K. Yuzuru, and W. Kazuhiro, 2012, "A Study on Propagation Characteristics of Spread Spectrum Sound Waves using Band-limited Ultrasonic Transducer", Journal of Robotics and Mechatronics, pp. 333-341.
7. A. Suzuki et al., 2009, "Measurement Accuracy on Indoor Positioning System Using Spread Spectrum Ultrasonic Waves", 4th International Conference on Autonomous Robots and Agents, Wellington, New Zealand, pp. 294-297.
8. A. Suzuki, I. Taketoshi and K. Watanabe, 2011, "A Performance Comparison of Measurement Distance between OOK and SS Modulation for Indoor Positioning Using Ultrasonic Transducers", IEEE Sensors, Limerick, Ireland, October, Open Poster.
9. A. Suzuki, I. Taketoshi and K. Watanabe, 2012, "Real-Time Distance Measurement for Indoor Positioning System Using Spread Spectrum Ultrasonic Waves", in Ultrasonic Waves. University Campus STeP Ri Slavka Krautzeka 83/A 51000, Rijeka, Croatia: INTECH, pp. 173-188.
10. P. Misra and P. Enge, 2001, Global Positioning System Signals, Measurements and Performance. Lincoln, MA 01773: Ganga-Jamuna Press.